Fast Isothermal Solidification During Transient Liquid Phase Bonding of a Nickel Alloy Using Pure Copper Filler Metal: Solubility *vs* Diffusivity

ALI GHASEMI and MAJID POURANVARI

This investigation aims at understanding the underlying fundamentals of the isothermal solidification phenomenon during the transient liquid phase (TLP) bonding process. The isothermal solidification is governed by solid-state diffusion of the melting point depressant (MPD) into the base material, which, in turn, is controlled by both kinetic and thermodynamic parameters; however, the latter factor is generally ignored. In this work, the competition between kinetics and thermodynamics of diffusion were considered in TLP bonding of a nickel alloy, Monel 400, using two distinct filler metals including pure copper (Cu) and Ni-Si-B filler metal. The joint generated by Ni-Si-B filler metal exhibited two key features including the presence of eutectic-type solidification products, an indication of incomplete isothermal solidification, and the presence of liquated grain boundaries in the substrate. However, the joint generated using pure Cu filler metal exhibited neither liquated grain boundaries nor precipitates in the diffusion-affected zone (DAZ). Interestingly, a fast isothermal solidification was observed when bonding using Cu filler metal. Despite the lower diffusivity of Cu, as a substitutional MPD in Ni-base substrate, compared to that of B, as an interstitial MPD, its higher solid solubility in the substrate provides a larger thermodynamic driving force for diffusion-induced isothermal solidification. Moreover, due to the high partitioning ratio of Cu in the Ni-base substrate and, hence, the lower difference between MPD solubility in liquid and solid phases, the required number of MPD atoms that should diffuse from the liquid phase into the base metal (BM) to complete isothermal solidification is much lower than that of B-containing filler metals. Therefore, both diffusivity and solubility of the MPD element should be considered in filler metal selection for achieving a fast isothermal solidification during TLP bonding.

https://doi.org/10.1007/s11661-019-05149-5
© The Minerals, Metals & Materials Society and ASM International 2019

I. INTRODUCTION

TRANSIENT liquid phase (TLP) bonding is a nearly ideal bonding process in which a filler metal containing a melting point depressant (MPD), usually boron (B), silicon (Si), and phosphorous (P), is melted to join base materials, including single-crystal and polycrystalline superalloys, together.[1–5] It is generally accepted that the process is composed of three different stages: the dissolution of the base material, isothermal solidification, and homogenization.[6–10] The isothermal solidification stage during TLP bonding that plays a key role in achieving an intermetallic-free joint[11–14] is controlled by the solid-state diffusion of the MPD element into the base material.[15–17] Since the isothermal solidification is controlled by solid-state diffusion of the MPD element into the base material, the process is slow especially when the gap size is large.[18,19] The time required for isothermal solidification completion is, therefore, of primary interest when deciding whether any particular system is suitable for diffusion brazing.[20]

In order to reduce the bonding time, it is important to use filler metals enabling archiving faster isothermal solidification. That is why filler metals containing B as the MPD are extensively used in the TLP bonding process of the nickel-base alloys.[20–25] Boron, as an interstitial atom, possesses high diffusion kinetics in Ni-base alloys.[22] Therefore, depletion of B from the liquid phase seems to occur quickly and solidification seems to be over in a relatively short period of time. Not only diffusion kinetics but also thermodynamics of diffusion is essential to determine the completion time of isothermal solidification.[14,26,27] This means that isothermal solidification during bonding using a filler metal containing a lower diffusivity MPD but a higher

ALI GHASEMI and MAJID POURANVARI are with the Department of Materials Science and Engineering, Sharif University of Technology, 11365-9466 Tehran, Iran. Contact email: pouranvari@sharif.edu

Manuscript submitted October 11, 2018.
Article published online March 1, 2019

driving force of diffusion can be considered to be completed in a shorter time than that of a B containing filler metal.[27] Therefore, there is a competition between kinetics and thermodynamics of diffusion to determine the rate of isothermal solidification during TLP bonding. In this article, this competition is investigated for bonding of a Ni-based alloy, Monel 400, using a pure copper (Cu) filler metal and a Ni-Si-B (MBF-30) filler metal. Pure Cu filler metal is representative of a low diffusivity element with a high thermodynamic driving force for diffusion in Ni-based alloys, and B in Ni-Si-B filler metal is representative of a high diffusivity element with a low thermodynamic driving force for diffusion in Ni-based alloys. Therefore, TLP bonding behaviors of two systems, including Monel 400/MBF-30/Monel 400 and Monel 400/Cu/Monel 400, are investigated in this work. Before presenting and discussing the experimental results, the fundamental basis for isothermal solidification is reviewed and the roles of both kinetics and thermodynamics of the diffusion are highlighted.

II. FACTORS DETERMINING ISOTHERMAL SOLIDIFICATION TIME: KINETICS OF DIFFUSION *VS* THERMODYNAMICS OF DIFFUSION

The underlying principles involved in isothermal solidification can be simply described with the help of binary phase diagrams. Consider TLP bonding of Ni using two filler metals including Ni-B alloy and pure Cu. B and Cu play the role of MPD in the filler metals. Figures 1(a) and (b) show schematics of Ni-B and Ni-Cu phase diagrams, respectively. Points 1 and 2 in Figure 1 correspond to C_{FM} (initial concentration of MPD in the filler metal) and C_{BM} (initial composition of MPD in the base metal (BM)), respectively. The C_{FM} values for Ni-B and pure Cu filler metals are the eutectic composition of Ni-B (*i.e.*, 3.7 wt pct B) and 100 wt pct Cu, respectively. In both cases, the melting point of the filler metal (T_M) is less than the solidus temperature (T_S) of the base material. Thus, at the bonding temperature (T_B), which is set between T_M and T_S, just filler metal will melt, not the base material. After melting of the filler metal, a liquid with the chemical composition of C_{FM} is formed and comes into contact with the solid base material. According to the binary phase diagrams, this liquid is not in equilibrium with the solid base material. In order to establish thermodynamic equilibrium at the liquid/solid interface, the chemical composition of the liquid and solid at the interface must become C_L (equilibrium MPD concentration in the liquid phase at the solid/liquid interface) and C_S (equilibrium MPD concentration in the solid phase at the solid/liquid interface), respectively. Points 3 and 4 in Figure 1 correspond to C_L and C_S, respectively. Chemical composition evolution of the liquid phase from C_{FM} to C_L requires dilution of the liquid phase from the MPD atoms. In the other words, the concentration of the MPD atoms in the liquid phase should decrease from C_{FM} to C_L, which is possible by interdiffusion of base material atoms into the liquid phase and MPD atoms

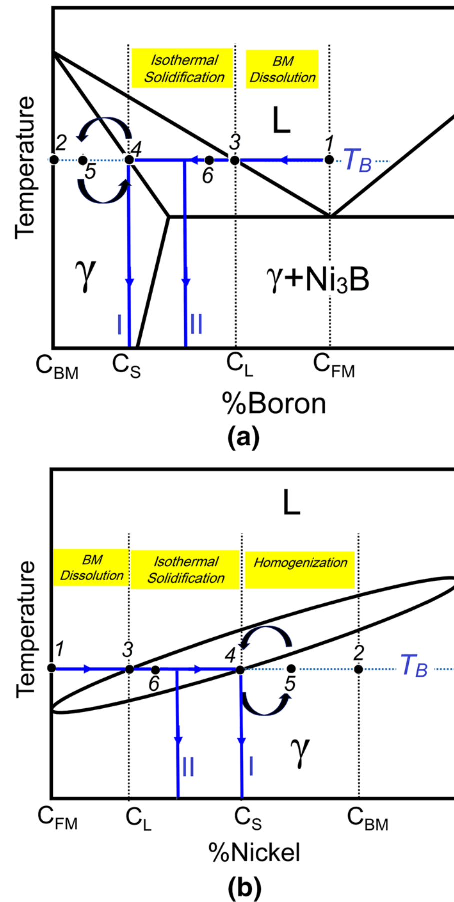

Fig. 1—Mechanism of isothermal solidification during TLP bonding of Ni using Ni-B and Cu filler metals with the help of schematic binary phase diagrams of (*a*) Ni-B and (*b*) Ni-Cu. C_{FM} (point 1) and C_{BM} (point 2) are the concentration of the MPD in the filler metal and BM, respectively. C_L (point 3) and C_S (point 4) are the equilibrium solubility of MPD in liquid and solid phases at the bonding temperature (T_B), respectively. Paths I and II are representative of the transformation path during isothermal and athermal solidification, respectively. The "deviation and re-establishment" of equilibrium at the interface is the driving force for the progress of isothermal solidification.

into the base material. Therefore, dissolution of the base material starts and reduces the fraction of MPD atoms to C_L in the liquid phase. On the other hand, by diffusion of MPD atoms from the liquid phase into the base material, the chemical composition of the solid phase at the interface changes to C_S. At this time, dissolution of base material ends. The duration of this step is usually considered to be short.[7,9,20,28]

After achieving equilibrium at the solid/liquid interface, isothermal solidification starts with the following mechanism. If the interface remains at the thermodynamic equilibrium conditions, isothermal solidification of the liquid phase never happens. In other words, the liquid and solid phases are in a stable condition, and if the equilibrium thermodynamics of the system at the interface remains unchanged, the liquid phase remains unchanged as well. Therefore, the reason for isothermal solidification of the liquid layer is deviation and re-establishment of equilibrium conditions at the interface. As mentioned earlier, the chemical compositions of

the liquid and solid phases in the equilibrium conditions are C_L and C_S, respectively, and they are required to be satisfied only at the interface. However, in most cases, the chemical composition of liquid is C_L all over the liquid. Still, it is C_S just at the interface in the solid phase. Because of the concentration gradient of MPD atoms between the interface and bulk of the solid phase, MPD atoms experience a solid-state diffusion toward the bulk of the base material. By the diffusion of MPD atoms, the interface of the solid base material is not C_S anymore and deviation from thermodynamic equilibrium takes place. This means that the composition of the solid phase at the interface changes from C_S at point 4 to 5. In order to re-establish the equilibrium conditions, MPD atoms diffuse from the liquid to the solid base material at the interface again to provide an equilibrium composition of C_S at the interface. By MPD atoms leaving the liquid, the liquid phase enters the two-phase region from point 3 to 6. This means that a small amount of liquid phase undergoes the solidification process. At this point, the remaining liquid's chemical composition is C_L and the chemical composition of the solid base material at the interface is C_S. In other words, after solidification of a small portion of the liquid phase, a new interface is formed, which is in equilibrium with the remaining liquid phase. This process of deviation and re-establishment of equilibrium continues to happen repeatedly until the last portion of the liquid phase solidifies. At this point, the isothermal solidification terminates. This definition of isothermal solidification can be helpful in finding the missing parameters affecting the isothermal solidification time. Based on the preceding discussion, the driving force of isothermal solidification is the continuous changing from stable to unstable conditions, which is caused by solid-state diffusion of MPD atoms from the interface toward the bulk of the base material. Therefore, by controlling the factors affecting solid-state diffusion, the isothermal solidification time can be controlled.[28–30]

As mentioned previously, the rate of isothermal solidification is controlled by the solid-state flux of MPD atoms into the bulk of the solid phase, which, in turn, is a function of the kinetics (diffusivity) and diffusion thermodynamics of MPD atoms. Although the thermodynamics of diffusion plays a key role in dictating the isothermal solidification time, it is generally an ignored factor in much of discussion about TLP bonding. As a general rule, the greater the atomic flux of the MPD atoms from the interface toward the bulk of the solid phase, the lesser the isothermal solidification time. According to first Fick's law (Eq. [1]), the atomic flux (J) is a function of the concentration gradient ($\partial C/\partial X$) as well as diffusivity (D):[31]

$$J = D_S \frac{\partial C}{\partial y} \quad [1]$$

By solving Fick's second law (Eq. [2]) at a boundary condition of $C(0,t) = C_S$ and initial condition of $C(y,0) = C_{BM}$, the concentration profile of the MPD atoms, $C(y,t)$, in the solid phase (base material) can be obtained as Eq. [3]:[8]

$$\frac{\partial C}{\partial t} = D_S \frac{\partial^2 C}{\partial y^2} \quad [2]$$

$$C(y,t) = C_S + (C_{BM} - C_S)\mathrm{erf}\left(\frac{y}{\sqrt{4D_S t}}\right) \quad [3]$$

By derivation of Eq. [3] with respect to y and substitution in Eq. [1], the atomic flux (J) can be calculated at the interface using Eq. [8]:

$$J = -\frac{\sqrt{D_S}(C_S - C_{BM})}{\sqrt{\pi t}} \quad [4]$$

It is worth noting that Eq. [4] is valid for the atomic flux into the solid phase at the stationary interface. Actually, it is not the case of TLP; however, it can be useful to show the underlying principle of solid-state diffusion during isothermal solidification. According to Eq. [4], there are two key factors controlling the MPD atomic flux during TLP bonding, as follows.

(1) Kinetics of diffusion; diffusivity of MPD in the BM: MPD atoms with a higher diffusion coefficient result in higher atomic flux and lower isothermal solidification time. The diffusion coefficient is a function of the nature of the MPD atom and the base material. Generally, an interstitial atom (*e.g.*, B in Ni) diffuses faster than a substitutional atom (*e.g.*, Cu in Ni).[31] Figure 2 illustrates schematically the effect of MPD diffusivity on atomic flux at constant C_S and C_{BM} amounts. In case A, the diffusivity coefficient (D_A) of the MPD atoms is more than the diffusivity coefficient of the MPD atoms in case B. This higher diffusivity causes more atoms to

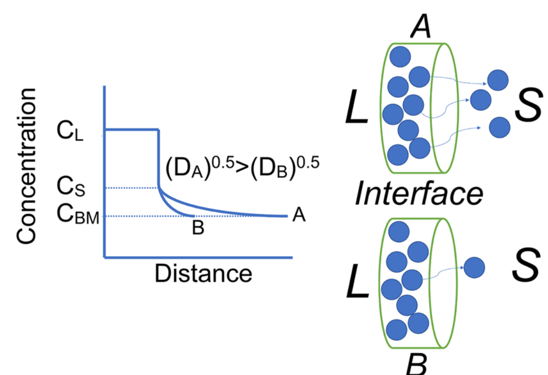

Fig. 2—Schematic of the effect of the kinetics of diffusion (MPD diffusivity) on solid-state atomic flux from the interface toward the bulk. A and B are MPD elements in the filler metal. The diffusion coefficient of A (D_A) is higher than the diffusion coefficient of B (D_B). Higher diffusivity causes faster diffusion and shallower concentration gradient.

diffuse from the interface toward the base material per unit time and, hence, results in a faster isothermal solidification.

(2) Thermodynamics of diffusion; solid solubility of MPD in the BM: The concentration difference between the interface (C_S) and the bulk of the base material (C_{BM}) is representative of the thermodynamics of diffusion or the driving force behind the diffusing atoms. The greater the concentration difference between the interface and the bulk, the greater the tendency of the MPD atoms to diffuse (*i.e.*, higher diffusion flux, J) and the lesser the isothermal solidification time. In most of the cases, for example, in the case of TLP bonding of nickel-base superalloys using B-containing filler metals, $C_{BM} = 0$. Therefore, the higher solid solubility of MPD in the BM (C_S) determines the degree of driving force for diffusion. This finding means that the higher equilibrium solubility limit of MPD atoms at the solid phase interface causes faster isothermal solidification. Generally, the solubility limit of interstitial atoms (*i.e.*, B) is far less than that of many substitutional atoms (*i.e.*, Cu) in Ni-based alloys.[27, 32] Figure 3 illustrates schematically the effect of thermodynamics of diffusion on the atomic flux at constant diffusivity (D). The higher driving force causes more atoms to diffuse from the interface toward the base material per unit time and, hence, results in a faster isothermal solidification.

In addition to the flux of MPD atoms, another factor that affects isothermal solidification is the number of MPD atoms that should diffuse from the liquid phase to the solid phase for complete isothermal solidification, which is a function of two distinct parameters, including the following.

(1) The concentration difference between the equilibrium composition of the liquid and solid phases ($C_L - C_S$): Isothermal solidification is accomplished when the last portion of the liquid phase with the composition of C_L at the centerline converts to the solid phase with the chemical composition of C_S.[8] According to the phase diagram, when the distance between the equilibrium composition of liquid and solid phases is long, more MPD atoms should diffuse to result in complete isothermal solidification. If the amount of J is constant for two different systems, the one with higher ($C_L - C_S$) experiences a longer isothermal solidification stage. This means that the higher portioning ratio of the MPD in the BM (*i.e.*, $k = C_S/C_L$) prompted isothermal solidification.[20,27]

(2) Thickness of the filler metal (W_0): By considering the case that $C_{BM} = 0$, just the filler metal is introducing MPD atoms into the liquid phase. It is obvious that a thicker filler metal has more MPD atoms compared to a thinner micrometers filler metal and needs more time for complete isothermal solidification.[19]

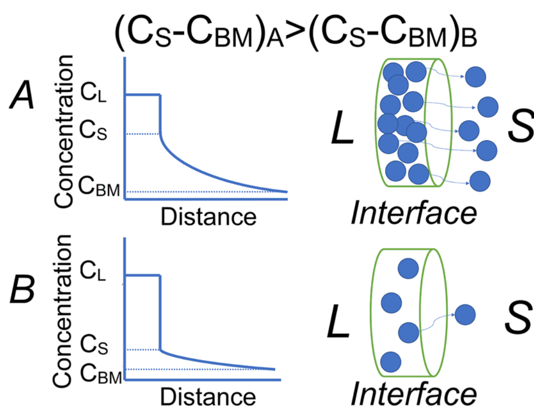

Fig. 3—Schematic of the effect of thermodynamics of diffusion (concentration gradient) on solid-state atomic flux from the interface toward the bulk. The MPD concentration gradient in the solid phase is $C_S - C_{BM}$. TLP bonding system A exhibited higher thermodynamic driving force (higher $C_S - C_{BM}$) compared to system B. This causes faster diffusion and steeper concentration gradient compared to system B.

In addition to the factors discussed previously, there are other factors that influence the isothermal solidification time, which are not applicable to this article. For example, (1) bonding temperature, which affects the maximum liquid phase width, the liquid phase composition, and MPD solubility;[14,32–36] (2) BM grain size, which can affect the grain boundary diffusion of the MPD;[29,37] (3) *in-situ* precipitation of the BM-MPD compounds during liquid phase disappearance, which can consume the MPD atoms and change the concentration gradient in the solid phase;[38] (4) liquid state diffusion of MPD atoms from one interface to the other side during dissimilar diffusion brazing, which can increase the gap size during isothermal solidification;[8] and (5) temperature gradient.[39] It is worth mentioning that the isothermal solidification rate is not constant during the TLP process, and it shows a parabolic behavior between solid liquid interface migration and processing time, which can be deviated in some cases based on the gap size and solubility limit of MPD atoms in the base material.[40]

The higher thermodynamics of diffusion in the Ni-Cu system with low kinetics and the higher kinetics of diffusion in the Ni-B system with low thermodynamics make the isothermal solidification challenging in these two systems. This article aims at investigating the competition between the kinetics and thermodynamics of diffusion in these two bonding systems

III. MATERIALS AND EXPERIMENTAL PROCEDURES

In this investigation, Monel 400 was used in the anneal condition as the base material. The chemical composition of Monel 400 was validated by spark emission spectroscopy. Commercial Ni-Si-B alloy (MBF-30) in the form of amorphous foil and pure Cu foil with a thickness of 50 μm were inserted as the filler

metals. Table I shows the chemical composition of the base material, the nominal composition of the filler metals, and the melting range of the filler metals.

The sizes of the BM test coupons, which were sectioned by a guillotine, were 10 mm × 10 mm × 2 mm. In order to remove the oxide films from the mating surfaces of the coupons, they were polished using 800-grade SiC paper. Foils were sectioned by a nibbler's tool to a size of 12 mm × 12 mm × 50 μm, and the sectioned foils were ultrasonically cleaned in an acetone bath. Sectioned pure Cu filler metals were used in the as-received condition. Then, they were inserted between two base material coupons. A stainless steel fixture was used to hold the gap size fixed and to apply bonding pressure. Figure 4 shows the schematic of the bonding sandwich. TLP bonding was carried out in a vacuum furnace under a vacuum of approximately 10^{-4} mbar. In order to compare the isothermal solidification completion time in the case of Monel 400/MBF-30/Monel 400 with Monel 400/Cu/Monel 400, the bonding temperature was fixed at 1393 K (1120 °C) and the bonding time at 10 minutes. The heating rate was 20 °C/min, which is a typical heating rate for industrial vacuum furnaces. In both cases, the liquid phase formed within the joint gap at the bonding temperature. This was evidenced by observation of the melting of the extra part of the interlayer on the external surface of the test coupons. Therefore, metallurgical bonds were formed in both cases based on the formation of a liquid/solid interface.

Bonded samples were sectioned in the direction of thickness and mounted in Bakelite. Then, they were polished and etched in 5 g $FeCl_3$, 2 mL HCl, and 96 mL methanol solution. Optical microscopy and field-emission scanning electron microscopy (FESEM) were used for the purpose of microstructural investigations on the sectioned samples. Semiquantitative chemical analyses of phases formed in the brazed affected zone were conducted using a TESCAN MIRA3 field-emission scanning electron microscope equipped with an ultra-thin window energy-dispersive X-ray spectrometer (EDS).

IV. RESULTS

A. *Microstructure of Monel 400/Ni-Si-B/Monel 400 Bond*

Figures 5(a) and (b) show the microstructure of the Monel 400/Ni-Si-B/Monel 400 bond. The dotted lines in Figure 5(b) show the approximate size of the solidification zone (SZ) where solidification is formed *via* two different mechanisms: isothermal solidification in which a single-phase solid solution is formed and athermal solidification in which solidification occurs *via* a eutectic-type reaction during cooling. Excessive grain growth and grain boundary liquation are the key feature phenomena in the base material.

The presence of eutectic-type solidification products at the joint centerline suggests that the disappearance of the liquid phase was not completed isothermally and the remaining liquid experienced athermal solidification. According to the schematic Ni-B binary phase diagram (Figure 1(a)), the residual liquid undergoes a eutectic reaction athermally (path II in Figure 1(a)) and the outcome of this reaction is a two-phase microstructure, which can be separated from the single-phase microstructure of the isothermal SZ (ISZ, path I in

Table I. Chemical Composition and Melting Temperature Range of Base Material and the Filler Metals

Material	Composition (Wt Pct)	Melting Temperature Range	
		Solidus [K (°C)]	Liquidus [K (°C)]
Monel 400	Ni-33.56Cu-1.88Fe-0.98Mn-0.13C-0.12Si	1573 (1300)	1623 (1350)
MBF-30	Ni-3.2B-4.5Si	1257 (984)	1327 (1054)
Pure Cu	99.9Cu	1356 (1083)	1356 (1083)

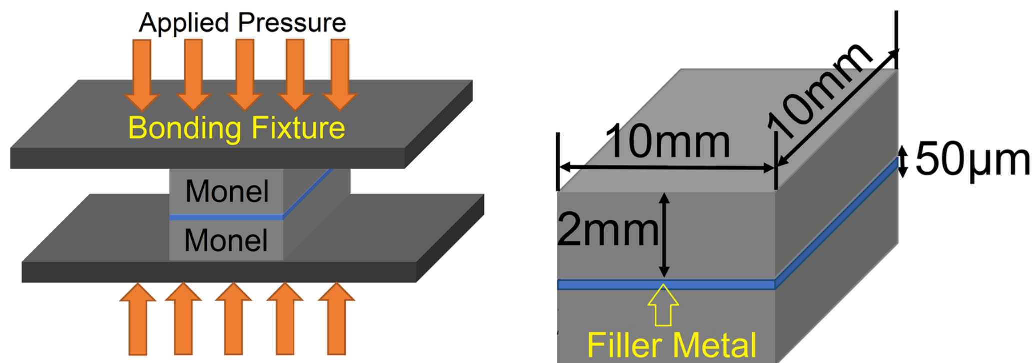

Fig. 4—Schematic of the TLP bonding system used in this investigation: Monel 400 nickel alloys were bonded using two different filler metals including pure Cu and Ni-Si-B (MBF30).

Figure 1(a)). Therefore, in the case of the MBF-30 interlayer, isothermal solidification is not completed after 10 minutes.

Figure 6 shows SEM micrographs detailing the microstructure of the bond region. Table II shows the chemical composition of the phases formed in the joint

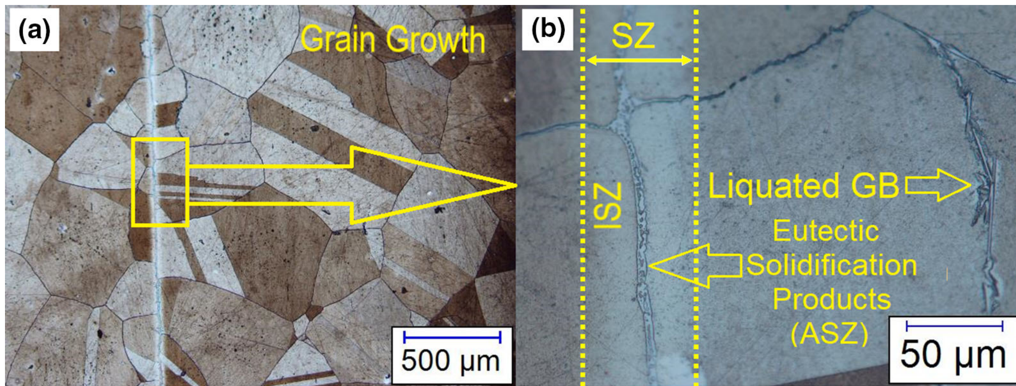

Fig. 5—(*a*) Microstructure of the Monel 400/Ni-Si-B/Monel 400 TLP bond showing the joint region and the extensive grain growth in the BM and (*b*) higher magnification of the joint region.

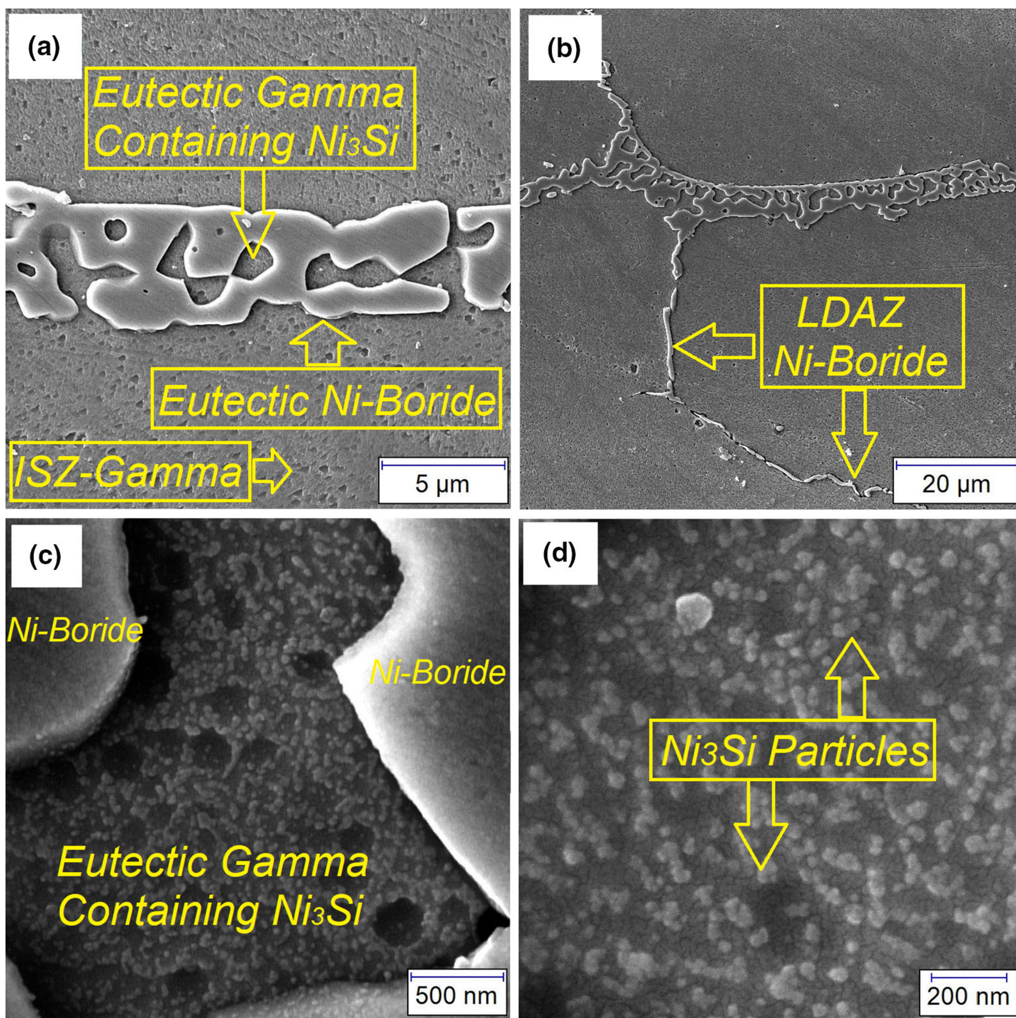

Fig. 6—SEM micrographs showing details of joint microstructure in Monel 400/MBF30/Monel 400: (*a*) eutectic constituents of athermal solidification (gamma solid solution and Ni-Boride) and ISZ, (*b*) liquated grain boundaries detected as Ni-boride, and (*c*) and (*d*) solid-state precipitation of Ni_3Si during the cooling stage.

Table II. Chemical Composition (Atomic Percent) of the Microconstituents Formed in the Bonding Affected Zone in the Bonding of Monel 400 Using MBF-30 Filler Metal

Sample	Microconstituents/Element	Ni	Cu	Si
Monel 400/MBF-30/Monel 400	eutectic Ni-B*	96.56	3.44	0
	ISZ-γ	74.07	22.00	3.96
	eutectic γ containing Ni3Si**	79.13 ± 0.86	13.26 ± 0.74	7.6 ± 0.59
	Ni-B in liquated grain boundaries*	94.08	4.68	1.24

*B was detected in this phase, although its concentration could not be determined with sufficient accuracy due to difficulty in quantifying light elements by the EDS analysis technique.
**The average composition of the various points within the eutectic γ containing Ni_3Si is reported.

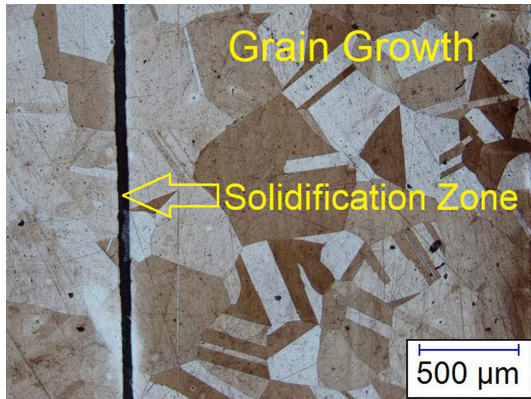

Fig. 7—Microstructure of the Monel 400/Cu/Monel 400 TLP bond. The dark-etching region is the ISZ. Excessive grain growth in the BM is evident.

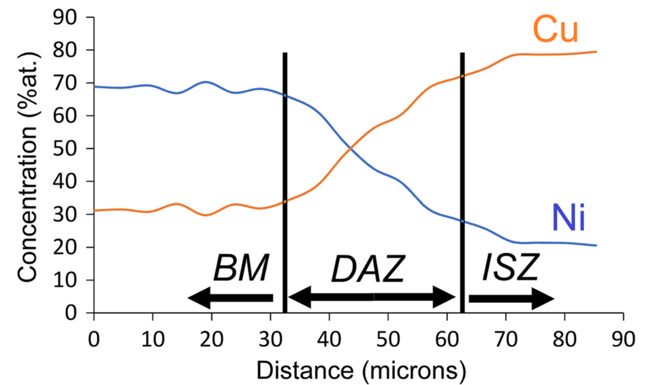

Fig. 8—X-ray line scan across the Monel 400/Cu/Monel 400 joint. The Cu concentration in the ISZ is lower than the solid solubility of Cu in BM (93.1 at. pct), which indicates that isothermal solidification is completely accomplished. DAZ and BM can be distinguished according to the line scan results.

region obtained *via* EDS-FESEM analysis. The analysis suggests that the ISZ is composed of a Ni-Cu-Si solid solution phase. Figure 6(a) shows that eutectic solidification products formed in the joint centerline (*i.e.*, ASZ) consisted of two phases including a solid solution phase and an intermetallic phase. Boron was detected in the intermetallic phase, although its concentration could not be determined with sufficient accuracy due to difficulty in quantifying light elements by the EDS analysis technique. Therefore, according to Table II, the intermetallic phase formed in the ASZ is a Si-free nickel-rich boride.

It is of note that no solid-state precipitation was observed in the BM. However, according to Figures 5(b) and 6(b), the grain boundaries in the BM were decorated by a continuous layer of intermetallic phase. EDS-FE-SEM confirmed that the intermetallic phase at the grain boundaries is a nickel-rich boride. Diffusion of B toward the base material caused the formation of liquated grain boundaries. The liquation phenomenon in this bonding system is discussed later in this article.

It is worth mentioning that no silicide was formed at the joint centerline during athermal solidification of the liquid phase. However, according to Figures 6(c) and (d), at higher magnifications, very fine precipitates were detected in the eutectic gamma phase. According to Table II, the Si content of the eutectic gamma is higher than that of the ISZ. Therefore, it can be inferred that these precipitates are Ni_3Si, as observed in previous works.[5,18,21,23,25,41]

B. *Microstructure of the Monel 400/Cu/Monel 400 Bond*

Figure 7 illustrates the microstructure of the Monel 400/Cu/Monel 400 TLP bond. The dark-etching region is the SZ of the bond. According to the Ni-Cu phase diagram, regardless of whether isothermal solidification happens, it is expected to obtain a single-phase solid solution microstructure at the joint centerline (consider paths I and II). There are no eutectic constituents as a witness of athermal solidification, as in the case of MBF-30. On the other hand, there is no evidence to determine the extension of the diffusion-affected zone (DAZ) because there is no liquated or precipitated phase near the joint. Therefore, it is not possible to distinguish ISZ, ASZ, DAZ, and BM from each other. In these circumstances, the chemical composition of the bonded joint can clarify whether the isothermal solidification was completed. According to Figure 1(b), achieving C_S at the joint centerline after solidification of the last portion of the liquid phase indicates that isothermal solidification is completed (path I). Figure 8 shows the X-ray line scan across the Monel 400/Cu/Monel 400 TLP bond. According to Figure 8, Cu concentration at the joint centerline is 79.5 at. pct, which is well below the C_S (*i.e.*, 93.1 at. pct Cu[42]) in the ISZ. Therefore, isothermal solidification is accomplished completely at this bonding condition. It is of note that not only isothermal solidification is accomplished, but also homogenization has occurred to some extent. The Cu content of the joint centerline is higher than the base

materials and that is why the joint centerline appears dark in the optical micrographs. It is worth mentioning that by means of the X-ray line scan, the DAZ can be distinguished from the BM. Therefore, it can be concluded that the isothermal solidification rate during TLP bonding of Monel 400 using pure Cu filler metal is higher than that using the MBF-30 filler metal.

V. DISCUSSION

A. *Solidification of the Liquid Phase in Monel 400/Ni-Si-B/Monel 400*

During isothermal solidification, B diffuses into the base material. If the B concentration in the entire liquid phase changes from C_L to C_S, complete isothermal solidification occurs (path I, Figure 1(a)). Otherwise, a portion of the liquid phase experiences athermal solidification during the cooling stage (path II, Figure 1(a)). The characteristic of this region is the presence of IMC compounds. Despite the fact that in many superalloys, such as Hastelloy X[41] and Inconel 718,[5] ternary eutectic constituents were reported in ASZ using MBF-30 filler metal, they are not the same as the product of athermal solidification in Monel 400 alloy. Pouranvari et al. provided the following solidification sequence for the Inconel 718/MBF-30/Inconel 718:[5]

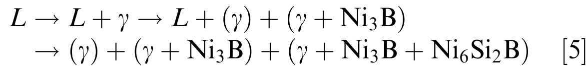

$$L \rightarrow L + \gamma \rightarrow L + (\gamma) + (\gamma + Ni_3B) \rightarrow (\gamma) + (\gamma + Ni_3B) + (\gamma + Ni_3B + Ni_6Si_2B) \quad [5]$$

The first step is the formation of primary gamma (γ) in the liquid phase. During the formation of primary gamma, B and Si segregate into the liquid phase but, of course, solubility of the Si in the primary gamma is much more than B and, therefore, the remaining liquid is enriched with a significant amount of B and a small amount of Si. In the next step, the binary eutectic reaction occurs. As the boride phases are Si free, the formation of Ni_3B causes the enrichment of the remaining liquid with Si, while there is still B in the liquid phase, and finally ternary eutectic reaction takes place.[5] However, in the case of Monel 400/MBF-30/Monel 400, the third step of the mentioned reaction does not happen and the solidification sequence is as follows (path II in Figure 1(a)):

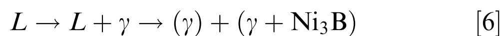

$$L \rightarrow L + \gamma \rightarrow (\gamma) + (\gamma + Ni_3B) \quad [6]$$

It is worth mentioning that there is no ternary eutectic product in the ASZ in the present system. According to the preceding discussion, if the remaining liquid does not become enriched with the Si atoms, ternary eutectic cannot happen. The initial amount of Si in the MBF-30 filler metal is 7.9 at. pct. By considering Table II, the amount of Si in the binary eutectic gamma is 7.6 ± 0.59 at. pct. This finding means that the binary eutectic gamma could solve a large amount of Si during the binary eutectic reaction and, therefore, the amount of Si in the remaining liquid cannot reach the ternary eutectic composition. That is why ternary constituents are not visible in the ASZ. It of note that the formation of brittle boride phases in the ASZ can provide a low fracture toughness that significantly decreases the load carrying capacity of the joint.[5] Therefore, there is a need to eliminate this phase *via* prolonged bonding time to achieve a bond with complete isothermal solidification.

B. *Solid-State Evolutions in Monel 400/Ni-Si-B/Monel 400*

As mentioned previously, the eutectic-γ contains a substantial amount of nanosized precipitates. Considering the morphology and size of these precipitates (averaged at 50 nm), it can be concluded that the formation of this phase occurred as solid-state precipitation during the cooling stage, not directly during solidification of the remaining liquid in the joint gap. According to EDS-FESEM, the eutectic-γ zone exhibited high Si content. Therefore, these precipitates can be assumed as Ni-rich silicides. The formation of these precipitates has been reported in previous works.[5,23,41] The reduction of solid solubility of Si in the γ phase during cooling causes the ejection of additional Si from supersaturated γ and subsequent solid-state precipitation of Ni-rich silicides. It is interesting to note that unlike the intermetallic phases formed during athermal solidification, which formed interlinked networks, these precipitates would not be expected to have detrimental effects on joint mechanical strength due to their nanosized dimensions and discrete morphology.

C. *Grain Boundary Liquation in the Monel 400/MBF30/Monel 400 Bond*

As mentioned previously, grain boundary liquation was detected in the substrate region of the Monel 400/MBF30/Monel 400 bond. Figures 5(b) and 6(b) show the liquated path along the grain boundaries in the base material. Gale and Wallach showed that during TLP bonding of the pure nickel substrates using MBF-30 filler metal, when the bonding temperature is above the Ni-B binary eutectic temperature, grain boundary liquation takes place instead of boride precipitation.[43,44] According to the fact that B diffusion into the base material controls the isothermal solidification in MBF-30 filler metal,[5] this statement is reasonable and, at bonding temperature [1393 K (1120 °C)], formation of liquated grain boundaries is inevitable. It is also worth mentioning that, the substrate in this study is Ni-Cu instead of pure Ni. The eutectic temperature in the Cu-B binary system[45] [1286 K (1013 °C)] is lower than that in the Ni-B binary system [1366 K (1093 °C)]; thus, the presence of Cu in the substrate (Monel 400) has intensified this issue. By moving from the interface toward the bulk of the base material, the liquated path becomes narrower and narrower. This phenomenon can degrade the mechanical properties of the joint due to the formation of hard and brittle Ni-rich boride along the grain boundaries.

D. *DAZ in the Monel 400/Cu/Monel 400 Bond*

The DAZ in the Monel 400/Cu/Monel 400 system does not include microstructural features, such as precipitation of secondary phases (Cu is soluble in Ni in all concentrations) or grain boundary liquation, which can be detected by microscopy analysis. Again, chemical composition analysis can be helpful in finding the DAZ where the concentration of Cu in the BM is greater than the initial value. According to Figure 8, the width of this region in Monel 400 is about 30 μm.

E. *Grain Growth in the BM*

Image J software was used to calculate the average grain size based on the intercept method before and after bonding. Excessive grain growth was observed in the base material after bonding. Figure 9 represents the microstructure of the BM before and after bonding. The average grain size was increased from 20 ± 4 to 480 ± 188 μm after bonding.

F. *Fast Isothermal Solidification Using Cu Filler Metal*

The isothermal solidification time during TLP bonding of Monel 400 using Cu filler metal is lower than that of MBF-30. This interesting result means that diffusivity of the MPD atoms is not the only controlling parameter and the thermodynamics of diffusion and the amount of diffusing MPD atoms are important as well. This result is mathematically verifiable by use of the atomic flux equation, as follows: Monel 400 is an approximately binary alloy mainly composed of Cu and Ni. Therefore, the binary Ni-Cu phase diagram can be accurately useful in finding the thermodynamic parameters. According to the Ni-Cu binary phase diagram, C_S = 93.1 at. pct Cu, C_L = 95 at. pct Cu at the bonding temperature, 1393 K (1120 °C),[42] and C_{BM} = 32 at. pct Cu. The diffusion coefficient of Cu and B in the base material (D) is given by Eq. [7]:[25]

$$D = D_0 \exp\left(\frac{-Q}{RT}\right) \quad [7]$$

The diffusion of MPD in Monel 400 can be approximated with enough accuracy with diffusion in pure nickel. (In the periodic table, Cu is next to nickel and it is almost the same in atomic size. Therefore, Cu sits as a substitutional atom in the lattice points of nickel crystals and does not change the lattice parameter and crystal structure as well. Consequently, the activation energy (Q) for diffusion of Cu and its frequency factor (D_0) in Monel 400 are virtually equal to those of pure nickel.) The values of Q and D_0 in pure nickel are 258 kJ/mol and 0.57 cm^2/s, respectively.[46]

In filler metals, which contain two types of MPD elements, the element with higher diffusivity controls the isothermal solidification step.[5] For example, in MBF-30, B and Si are considered to be MPD elements. Since the diffusion coefficient of B in the solid solution nickel matrix is much higher than Si (the diffusion coefficients of B and Si in a nickel substrate are reported as $6.22 \times 10^{-11}\mathrm{m^2s^{-1}}$ and $3.09 \times 10^{-14}\mathrm{m^2s^{-1}}$ at 1373 K (1100 °C), respectively),[5] solid-state diffusion of B in the base material controls the isothermal solidification. Therefore, the isothermal solidification time of the Monel 400/MBF-30/Monel 400 system can be approximated by the binary Ni-B phase diagram. According to the Ni-B binary phase diagram, C_S = 0.3 at. pct B, C_L = 15.8 at. pct B at about 1393 K (1120 °C),[32,33] and C_{BM} = 0. The value of D for B diffusion into the Ni substrate is assumed to be $6.22 \times 10^{-11}\mathrm{m^2s^{-1}}$ at the bonding temperature.[43] The values of the diffusion coefficient D (kinetics of diffusion), $C_S - C_{BM}$ (thermodynamics of diffusion), and $C_L - C_S$ (number of diffusing atoms) are given in Table III.

According to the atomic flux relation (Eq. [4]) and by substituting the values presented in Table III, the B-to-Cu ratio of the MPD flux in the Ni substrate is

$$\frac{J_{\mathrm{Cu}\to\mathrm{Ni}}}{J_{\mathrm{B}\to\mathrm{Ni}}} = \frac{C_S^{\mathrm{Cu}} - C_{BM}^{\mathrm{Cu}}}{C_S^{\mathrm{B}} - C_{BM}^{\mathrm{B}}} \times \frac{\sqrt{D_{\mathrm{Cu}\to\mathrm{Ni}}}}{\sqrt{D_{\mathrm{B}\to\mathrm{Ni}}}} = 2.83 \quad [8]$$

Therefore, it is concluded that the Cu flux in Monel 400 is greater than B. In addition, the ($C_L - C_S$) values in the Ni-Cu and Ni-B systems are 1.9 at. pct Cu and

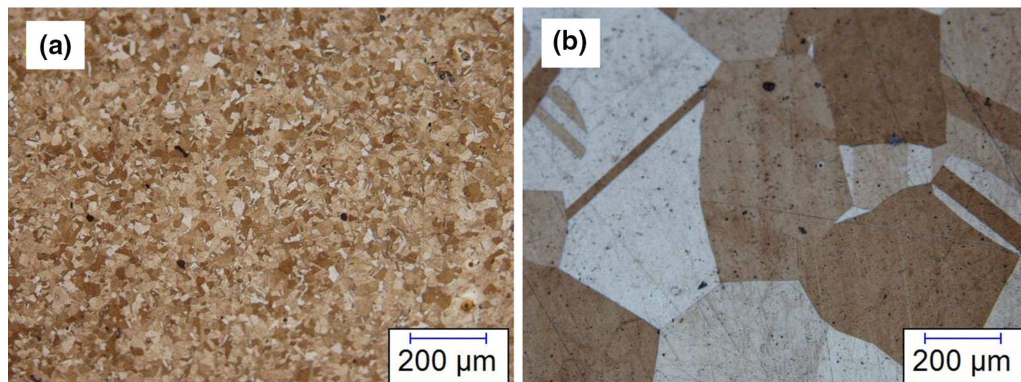

Fig. 9—Microstructure of the Monel 400 base material (*a*) before and (*b*) after TLP bonding at 1397 K (1120 °C) for 10 min. Excessive grain growth is evident in the substrate after bonding.

Table III. Comparison of Isothermal Solidification Parameters for TLP Bonding of Monel Using MBF-30 and Cu Filler Metals

Filler Metal	Diffusion Kinetics	Diffusion Thermodynamics	Number of Diffusing Atoms
MBF-30	$D_{B\rightarrow Ni} = 6.22 \times 10^{-10}$[35]	$C_S^B - C_{BM}^B = 0.3$at.pct	$C_L^B - C_S^B = 15.5$at.pct
Cu	$D_{Cu\rightarrow Ni} = 1.2 \times 10^{-14}$[38]	$C_S^{Cu} - C_{BM}^{Cu} = 61.1$at.pct	$C_L^{Cu} - C_S^{Cu} = 1.9$at.pct

15.5 at. pct B, respectively.[42] This finding means that in the case of MBF-30 filler metal, the amount of MPD atoms that must diffuse into the base material to finish the isothermal solidification is 8 times greater than in the case of pure Cu filler metal.

The higher atomic flux and lower number of diffusing atoms for isothermal solidification in the case of pure Cu filler metal cause faster isothermal solidification in the Monel 400/Cu/Monel 400 case. By consideration of both the atomic flux (J) and amount of required diffusing atoms, the isothermal solidification time in the case of Cu filler metal is roughly 23 times faster than that of the MBF-30 filler metal.

It is worth mentioning that Shinmura *et al.*[27] numerically compared the isothermal solidification time during TLP bonding of Ni using three different filler metals including Ni-B, Ni-P, and pure Cu. They found that the pure Cu filler metal exhibited faster isothermal solidification compared to the others. They related this finding to the higher partitioning ratio (*i.e.*, $K = C_S/C_L$) of Cu in Ni. They suggested that a higher partitioning ratio leads to a higher concentration gradient, which accelerates isothermal solidification. Indeed, they represented the partitioning ratio as a factor to determine the concentration gradient.[27] However, by considering the fact that the concentration gradient in the solid phase is the controlling factor in MPD flux into the base material, the partitioning ratio cannot express the concentration gradient in the solid phase. A high $K = C_S/C_L$ value does not necessarily suggest a higher concentration gradient for MPD diffusion in the base material. In fact, it is the $(C_S - C_{BM})$ value that governs the thermodynamics of diffusion.

It is of interest to comment on the width of the residual liquid in Monel 400/MBF-30/Monel 400. As discussed previously, the isothermal solidification time in the case of MBF-30 is expected to be roughly 23 times longer than that of pure Cu filler metal. However, according to Figure 5(b), after just 10 minutes, the level of isothermal solidification progress is high and the width of the ISZ is about 43 μm, meaning that only about 7 μm of the initial liquid phase remained at the joint region before the cooling stage. Therefore, it seems that the isothermal solidification time is less than what is predicted. To answer this contradiction, it should be considered that the represented calculations are based on B diffusion in solid Ni substrate. However, because of grain boundary liquation in Monel 400, liquid paths are formed for B diffusion and this results in a higher flux of MPD atoms and lower isothermal solidification time than expected. That is why after 10 minutes, a significant amount of liquid phase experienced isothermal solidification.

Finally, it should be noted that the filler alloy selection is a key issue during the design stage of the TLP process. In addition to the time required to complete isothermal solidification, the joint properties, including mechanical strength and corrosion resistance, should also be considered for commercial application of pure Cu for TLP bonding.

VI. CONCLUSIONS

Isothermal solidification during TLP bonding not only controlled by the kinetic parameters (*i.e.*, MPD diffusivity) but also thermodynamic parameters (*i.e.*, solubility and partitioning of MPD in the substrate) could play a pronounced role in determining the time required to complete isothermal solidification. This lesson can be understood by the TLP bonding of a Ni alloy (in the present case, Monel 400) using a pure Cu filler metal. Despite low diffusivity of Cu in the Ni-base substrate, bonding using a pure Cu filler metal exhibited a fast isothermal solidification compared to the bonding using a B-containing filler metal. The high solubility of Cu in Ni-base substrate provides a high deriving force for diffusion. In addition, its high partitioning ratio (*i.e.*, low difference between liquid solubility and solid solubility of MPD in the substrate) reduces the number of atoms that requires diffusing from the liquid into the base material to complete isothermal solidification, enhancing the rate of solidification. Therefore, it can be concluded that the thermodynamic parameters play a strong role in the isothermal solidification rate. To achieve fast isothermal solidification during TLP bonding, both diffusivity and solubility of the MPD should be considered in filler metal development.

REFERENCES

1. M Kapoor, ÖN Doğan, CS Carney, RV Saranam, P McNeff, and BK Paul: *Metall. Mater. Trans. A*, 2017, vol. 48A, pp. 3343–56.
2. OA Ojo: *J. Mater. Sci.*, 2012, vol. 47, pp. 1598–1602.
3. OA Idowu, OA Ojo, and MC Chaturvedi: *Metall. Mater. Trans. A*, 2006, vol. 37A, pp. 2787–96.
4. NC Sheng, JD Liu, T Jin, XF Sun, and ZQ Hu: *Metall. Mater. Trans. A*, 2013, vol. 44A, pp. 1793–1804.
5. M Pouranvari, A Ekrami, and AH Kokabi: *J. Alloy. Compd.*, 2013, vol. 563, pp. 143–49.
6. DS Duvall: *Weld. J.*, 1974, vol. 43, pp. 203–14.
7. WD MacDonald and TW Eagar: *Annu. Rev. Mater. Sci.*, 1992, vol. 22, pp. 23–46.
8. Y Zhou, WF Gale, and TH North: *Int. Mater. Rev.*, 1995, vol. 40, pp. 181–96.

9. WF Gale and DA Butts: *Sci. Technol. Weld. Join.*, 2004, vol. 9, pp. 283–300.
10. CW Sinclair: *J. Phase Equilibria*, 1999, vol. 20, p. 361.
11. M Khakian, S Nategh, and S Mirdamadi: *J. Alloy. Compd.*, 2015, vol. 653, pp. 386–94.
12. MA Arafin, M Medraj, DP Turner, and P Bocher: *Mater. Sci. Eng. A*, 2007, vol. 447, pp. 125–33.
13. NP Wikstrom, AT Egbewande, and OA Ojo: *J. Alloy Compd.*, 2008, vol. 460, pp. 379–85.
14. A Ghoneim and OA Ojo: *Mater. Charact.*, 2011, vol. 62, pp. 1–7.
15. M Pouranvari, A Ekrami, and AH Kokabi: *Can. Metall. Q.*, 2014, vol. 53, pp. 38–46.
16. OA Ojo, NL Richards, and MC Chaturvedi: *Sci. Technol. Weld. Join.*, 2004, vol. 9, pp. 532–40.
17. M Pouranvari, A Ekrami, and AH Kokabi: *J. Alloy Compd.*, 2009, vol. 469, pp. 270–75.
18. M Pouranvari, A Ekrami, and AH Kokabi: *Mater. Sci. Technol.*, 2013, vol. 29, pp. 980–84.
19. OA Ojo, NL Richards, and MC Charturvedi: *Sci. Technol. Weld. Join.*, 2004, vol. 9, pp. 209–20.
20. GO Cook and CD Sorensen: *J. Mater. Sci.*, 2011, vol. 46, pp. 5305–23.
21. M Pouranvari, A Ekrami, and AH Kokabi: *J. Alloy. Compd.*, 2008, vol. 461, pp. 641–47.
22. F Jalilian, M Jahazi, and RAL Drew: *Mater. Sci. Eng. A*, 2006, vol. 423, pp. 269–81.
23. M Mosallaee, A Ekrami, K Ohsasa, and K Matsuura: *Metall. Mater. Trans. A*, 2008, vol. 39A, p. 2389.
24. S Steuer and RF Singer: *Metall. Mater. Trans. A*, 2014, vol. 45A, pp. 3545–53.
25. A. Ghasemi and M. Pouranvari: *Sci. Technol. Weld. Join.,* 2018, in press.
26. TC Illingworth, IO Golosnoy, and TW Clyne: *Mater. Sci. Eng. A*, 2007, vol. 445, pp. 493–500.
27. T Shinmura, K Ohsasa, and T Narita: *Mater. Trans.*, 2001, vol. 42, pp. 292–97.
28. J Ruiz-Vargas, N Siredey-Schwaller, N Gey, P Bocher, and A Hazotte: *J. Mater. Process. Technol.*, 2013, vol. 213, pp. 20–29.
29. A Ghoneim and OA Ojo: *Metall. Mater. Trans. A*, 2012, vol. 43A, pp. 900–11.
30. OA Ojo and O Aina: *Metall. Mater. Trans. A*, 2018, vol. 49A, pp. 1481–85.
31. DR Askeland and PP Phulé: *The Science and Engineering of Materials*, Brooks/Cole-Thomson Learning, Monterey, CA, 2003.
32. OA Idowu, NL Richards, and MC Chaturvedi: *Mater. Sci. Eng. A*, 2005, vol. 397, pp. 98–112.
33. NP Wikstrom, OA Ojo, and MC Chaturvedi: *Mater. Sci. Eng. A*, 2006, vol. 417, pp. 299–306.
34. R Bakhtiari, A Ekrami, and TI Khan: *Mater. Sci. Eng. A*, 2012, vol. 546, pp. 291–300.
35. RK Saha and TI Khan: *J. Mater. Eng. Perform.*, 2006, vol. 15, pp. 722–28.
36. B Abbasi-Khazaei, G Asghari, and R Bakhtiari: *Weld. J.*, 2016, vol. 95, pp. 68–76.
37. H Kokawa, CH Lee, and TH North: *Metall. Mater. Trans. A*, 1991, vol. 22A, pp. 1627–31.
38. M Pouranvari, A Ekrami, and AH Kokabi: *Sci. Technol. Weld. Join.*, 2018, vol. 1, pp. 13–18.
39. AG Bigvand and OA Ojo: *Metall. Mater. Trans. A*, 2014, vol. 45A, pp. 1670–74.
40. MM Abdelfatah and OA Ojo: *Metall. Mater. Trans. A*, 2009, vol. 40A, pp. 377–85.
41. A Ghasemi and M Pouranvari: *Sci. Technol. Weld. Join.*, 2018, vol. 23, pp. 441–48.
42. WG Moffatt: *The Handbook of Binary Phase Diagrams*, General Electric Co., Schenectady, NY, 1976, vol. 1–2.
43. WF Gale and ER Wallach: *Metall. Mater. Trans. A*, 1991, vol. 22A, pp. 2451–57.
44. S Steuer and RF Singer: *Metall. Mater. Trans. A*, 2013, vol. 44A, pp. 2226–32.
45. DJ Chakrabarti and DE Laughlin: *J. Phase Equilib.*, 1982, vol. 3, pp. 45–48.
46. JC Lippold, SD Kiser, and JN DuPont: *Welding Metallurgy and Weldability of Nickel-Base Alloys*, Wiley, New York, 2011.

Publisher's Note Springer Nature remains neutral with regard to jurisdictional claims in published maps and institutional affiliations.